

Bad-Metal Behavior Reveals Mott Quantum Criticality in Doped Hubbard Models

J. Vučičević,¹ D. Tanasković,¹ M. J. Rozenberg,² and V. Dobrosavljević³

¹*Scientific Computing Laboratory, Institute of Physics Belgrade, University of Belgrade, Pregrevica 118, 11080 Belgrade, Serbia*

²*Laboratoire de Physique des Solides, CNRS-UMR8502, Université de Paris-Sud, Orsay 91405, France and Departamento de Física, FCEN, Universidad de Buenos Aires, Ciudad Universitaria Pabellón I, (1428) Buenos Aires, Argentina*

³*Department of Physics and National High Magnetic Field Laboratory, Florida State University, Tallahassee, Florida 32306, USA*

(Received 26 December 2014; published 18 June 2015)

Bad-metal (BM) behavior featuring linear temperature dependence of the resistivity extending to well above the Mott-Ioffe-Regel (MIR) limit is often viewed as one of the key unresolved signatures of strong correlation. Here we associate the BM behavior with the Mott quantum criticality by examining a fully frustrated Hubbard model where all long-range magnetic orders are suppressed, and the Mott problem can be rigorously solved through dynamical mean-field theory. We show that for the doped Mott insulator regime, the coexistence dome and the associated first-order Mott metal-insulator transition are confined to extremely low temperatures, while clear signatures of Mott quantum criticality emerge across much of the phase diagram. Remarkable scaling behavior is identified for the entire family of resistivity curves, with a quantum critical region covering the entire BM regime, providing not only insight, but also quantitative understanding around the MIR limit, in agreement with the available experiments.

DOI: 10.1103/PhysRevLett.114.246402

PACS numbers: 71.27.+a, 71.30.+h

Metallic transport inconsistent with Fermi liquid theory has been observed in many different systems; it is often linked to quantum criticality around some ordering phase transition [1,2]. Such behavior is notable near quantum critical points in good conductors, for example in heavy fermion compounds [3,4]. In several other classes of materials, however, much more dramatic departures from conventional metallic behavior are clearly observed, where resistivity still rises linearly with temperature, but it reaches paradoxically large values, well past the Mott-Ioffe-Regel (MIR) limit [5,6]. This bad-metal (BM) behavior [7] was first identified in the heyday of high-temperature superconductivity, in materials such as $\text{La}_{2-x}\text{Sr}_x\text{CuO}_4$ [8]. While the specific copper-oxide family and related high- T_c materials remain ill-understood and marred with controversy, it soon became clear that BM behavior is a much more general feature [6] of materials close to the Mott metal-insulator transition (MIT) [9]. Indeed, it has been clearly identified also in various oxides [10,11], organic Mott systems [12–14], as well as more recently discovered families of iron pnictides [15]. Despite years of speculation and debate, so far its clear physical interpretation has not been established.

To gain reliable insight into the origin of BM behavior, it is useful to examine an exactly solvable model system, where one can suppress all possible effects associated with the approach to some broken symmetry phase, or those specific to low dimensions and a given lattice structure. This can be achieved by focusing on the maximally frustrated Hubbard model, where an exact solution can be obtained by solving dynamical mean-field theory (DMFT) equations [16] in the paramagnetic phase. Although various aspects of the DMFT equation have been studied for more than twenty years, only very recent work [17,18] established how to identify the quantum critical (QC) behavior

associated with the interaction-driven Mott transition at half-filling.

Here we present a large-scale computational study across the entire phase diagram, showing that qualitatively different transport behavior is found in doped Mott insulators. Our study reveals a clear and quantitative connection between BM phenomenology and the signatures of Mott quantum criticality, including the characteristic mirror symmetry [19] of the relevant scaling function. We demonstrate that the associated QC region, featuring linear temperature dependence of resistivity around the MIR limit, corresponds to a fully incoherent transport regime. In contrast, the coherent Fermi liquid (FL) regime and even the resilient-quasiparticle regime [20,21] do emerge at lower temperature, but here the resistivity remains well below the MIR limit. Our results provide strong evidence that bad-metallic behavior represents a universal feature of high-temperature transport close to the Mott transition, presenting intriguing parallels with recent ideas based on holographic duality [22,23].

Phase diagram.—We consider a single-band Hubbard model defined by the Hamiltonian

$$H = -t \sum_{\langle i,j \rangle, \sigma} (c_{i\sigma}^\dagger c_{j\sigma} + \text{H.c.}) + U \sum_i n_{i\uparrow} n_{i\downarrow} - \mu \sum_{i,\sigma} c_{i\sigma}^\dagger c_{i\sigma},$$

where t stands for the nearest-neighbor hopping amplitude, U is the on-site interaction, and μ denotes the chemical potential. The creation and annihilation operators for spin orientation σ are denoted by c_σ^\dagger and c_σ , and $n_{i\sigma} = c_{i\sigma}^\dagger c_{i\sigma}$. We solve the DMFT equations using the continuous-time quantum Monte Carlo (CTQMC) algorithm for the impurity solver [24–26]. We focus on the paramagnetic solution which is a physically justified assumption for frustrated lattices. We

use the semielliptic bare density of states and set the half-bandwidth $D = 1$ as the unit of energy. This corresponds to the infinitely dimensional Bethe lattice, as well as the fully connected lattice with random hopping amplitudes [16].

At half-filling, strong enough on-site interaction U opens a spectral gap at the Fermi level and produces the Mott insulating state [16]. The Mott insulator can also be destroyed by adding electrons to the system, i.e., raising the chemical potential μ . When μ reaches the upper Hubbard band, the system is once again conducting [20]. In both cases, at low temperature the transition is of the first order, and features a pronounced jump in the value of resistivity and other quantities [27]. Around the first-order transition line, a small coexistence region is present, where both metallic and insulating phases are locally stable. Our calculations show (see the Supplemental Material, Secs. I and II [28]) that the critical end-point temperature $T_c(U)$ for the doping-driven transition rapidly drops with increasing interaction, and at $U = 4$ it already is less than 10% of that at half-filling. This is illustrated in Fig. 1(a). At the critical end-point (red dots), the two solutions merge, and above it no true distinction between the phases exists; only a rapid

crossover is observed upon variation of U or μ . Previous work [17,18] examined the vicinity of the interaction-driven MIT at half-filling; here we analyze the broad finite temperature crossover region between the half-filled Mott insulator and the doped Fermi liquid state [27,34–36]. This bad-metal regime, displaying very different transport behavior than that found at half-filling, is the main focus of this work.

In Fig. 1(b), we color-code the resistivity in the (μ, T) plane, calculated for $U = 4$. The resistivity is given in units of the Mott-Ioffe-Regel limit ρ_{MIR} which is defined as the highest possible resistivity in a Boltzmann semiclassical metal, corresponding to the scattering length of one lattice spacing. Numerical value for ρ_{MIR} is taken consistently with Ref. [21]. At $\mu = U/2$, the system is half-filled. At approximately $\mu = U - D = 3$, the Fermi level enters the upper Hubbard band, and a first-order doping-driven MIT is observed at temperatures below $T_c = 0.003D$. While the chemical potential is within the gap, a clear activation behavior, $\rho \sim e^{E_g/T}$, is found at low temperatures. On the metallic side of the MIT, due to the strong electron-electron scattering, the resistivity grows rapidly with temperature, and typical Fermi-liquid behavior is observed only below rather low coherence temperature T_{FL} (denoted with the gray dashed line).

Quantum critical scaling.—In the standard scenario for quantum criticality [1,9], the system undergoes a zero-temperature phase transition at a critical value of some control parameter $g = g_c$, and within a V-shaped finite temperature region, physical quantities display scaling behavior of the form $A(g, T) = A_c(T)F[T/(g - g_c)^z]$. Mott MIT is a first-order phase transition [37], but the corresponding coexistence region is confined to extremely low temperatures, and at temperatures sufficiently above the critical end-point T_c , the quantum effects are expected to set in [1], and restore the QC behavior.

To test the QC scaling hypothesis in the case of a Mott transition, one must first identify the appropriate $g_c(T)$ instability trajectory [17,18] which enters the argument of the scaling function (for illustration, see the Supplemental Material, Fig. 2 [28]). $g_c(T)$ marks, on the phase diagram, a trajectory where the system is least stable (i.e., is found in equal proximity to both the metal and the insulator), and is therefore most prone to fluctuations. The relevant thermodynamic stability is most easily determined from the curvature λ of the free energy functional $\mathcal{F}[G(i\omega_n)]$ near its global minimum; this can be numerically determined by monitoring the convergence rate in the DMFT self-consistency loop [17]. Having in mind the analogy of this definition with the standard Widom crossover line for classical liquid-gas transitions [38], we refer to the instability line as the “quantum Widom line” (QWL) [18].

We carried out a careful λ analysis for the doped Mott insulator (see the Supplemental Material, Sec. III [28]), and we display the resulting QWL trajectory $\mu^*(T)$ as an orange line in all plots [throughout this Letter, an asterisk in the superscript indicates physical quantities evaluated along the

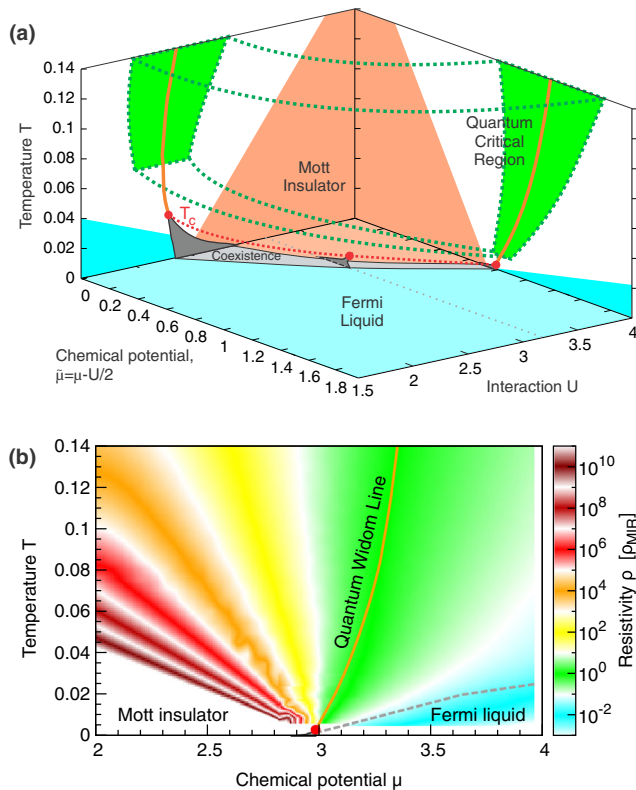


FIG. 1 (color online). (a) Phase diagram of the maximally frustrated Hubbard model. The quantum critical scaling is observed in the green region which extends to lower temperatures as T_c (red dots) is reduced. (b) Color plot of the resistivity in the (μ, T) plane for $U = 4$. The quantum Widom line (see text) passes through the crossover region where the resistivity is around the MIR limit. The coexistence region (gray) is barely visible on the scale of this plot.

QWL; e.g., $\rho^*(T)$ is resistivity calculated at temperature T at $\mu = \mu^*(T)$. The QC region (green) spreads above the critical end point (red points and dotted line) and quickly extends to much lower temperatures as T_c is reduced [Fig. 1(a)]. The QWL, separating the metalliclike and the insulatinglike behavior, marks the center of the corresponding QC region, where the resistivity curves are expected to display the scaling behavior of the form

$$\rho(\mu, T) = \rho^*(T)F[T/T_0(d\mu)]. \quad (1)$$

Here the parameter T_0 should assume power-law dependence on the deviation from the QWL: $T_0(d\mu) \sim d\mu^{z\nu}$, with $d\mu = \mu - \mu^*(T)$.

To check validity of the scaling hypothesis, Eq. (1), we calculate the resistivity along the lines parallel to the QWL, as shown in Fig. 2(a). We find that, for the doped Mott insulator, the resistivity shows very weak temperature dependence along the QWL. In particular, above $T = 0.08$, it follows the line of constant resistivity which coincides with the MIR limit, $\rho^*(T > 0.08) = \rho_{\text{MIR}}$ (in contrast to the behavior previously established at half-filling [17,18], where $\rho \gg \rho_{\text{MIR}}$ along the QWL). In fact, all curves converge precisely to the MIR limit at high temperatures, suggesting its fundamental role in characterizing the metal-insulator crossover for doped Mott insulators. The curves also display the characteristic bifurcation upon reducing temperature, and a clear change in trend upon crossing the QWL. The scaling analysis confirms that all the curves indeed display fundamentally the same functional dependence on temperature, and that they all can be collapsed onto two distinct branches of the corresponding scaling function [Fig. 2(b)]. The scaling exponent has been estimated to be $z\nu \approx 1.35 \pm 0.1$ for both branches of the

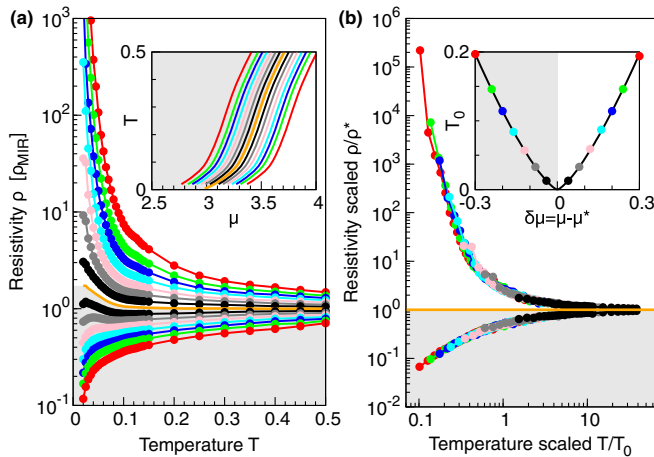


FIG. 2 (color online). (a) Family of resistivity curves calculated along lines parallel to the QWL (orange). (b) Upon rescaling the temperature with adequately chosen parameter T_0 , the resistivity curves collapse and reveal mirror symmetry of metalliclike and insulatinglike behavior around the QWL. T_0 depends on the distance from the QWL as $T_0(d\mu) \sim d\mu^{z\nu}$, with $z\nu \approx 1.35$.

scaling function, which display mirror symmetry [17,19] over almost two decades in T/T_0 , and the scaling covers more than 3 orders of magnitude in resistivity.

Bad-metal behavior.—We demonstrated the emergence of clearly defined quantum critical behavior through an analysis of the (μ, T) phase diagram, with $d\mu = \mu - \mu^*$ as the scaling parameter. From the experimental point of view, it is, however, crucial to identify the corresponding QC region in the (δ, T) plane and understand its implications for the form of the resistivity curves for fixed level of doping $\rho(T)|_\delta$. By performing a careful calculation of the $\delta(\mu, T)$ dependence (see the Supplemental Material, Fig. 4 [28]), it is straightforward to replot our phase diagram and resistivity curves in the (δ, T) plane. Remarkably, we find that the quantum critical scaling region covers a broad range of temperatures and dopings, and almost perfectly matches the region of the well-known bad-metal transport [21,39], characterized by the absence of long-lived quasiparticles and linear $\rho(T)|_\delta$ curves. We first analyze the (δ, T) phase diagram in detail, and then establish a connection between the slope of $\rho(T)|_\delta$ curves in the bad-metal regime and the QC scaling exponent νz .

In Fig. 3(a), we show the phase diagram of the doped Mott insulator. At $T = 0$, the Mott insulator phase is found exclusively at zero doping. At low enough temperature and finite doping, characteristic Fermi liquid behavior is always observed. Here, the resistivity is quadratic in temperature, while a clear Drude peak is observed at low frequencies in optical conductivity and density of states (see the Supplemental Material, Fig. 5 [28]). The coherence temperature T_{FL} is found to be proportional to the amount of doping δ , however, with a small prefactor of about 0.1, in agreement with Refs. [20,21]. In a certain temperature range above T_{FL} , a Drude peak is still present as well as the quasiparticle resonance in the single-particle density of states, but the resistivity no longer follows the FL T^2 dependence. This corresponds to the resilient-quasiparticle (RQP) transport regime, which was carefully examined in Ref. [21]. At even higher temperatures, the temperature-dependent resistivity at fixed doping $\rho(T)|_\delta$ enters a prolonged linear regime [see Fig. 3(b)] [40], which is accompanied by the eventual disappearance of the Drude peak around the MIR limit. This behavior is usually referred to as the bad-metal regime [21]. The resistivity is comparable to the MIR limit throughout the BM region, and the QWL (as determined from our thermodynamic analysis) passes through its middle.

The region of linear $\rho(T)|_\delta$ dependence is found to be completely encompassed by the QC scaling region between the dashed lines on Fig. 3(a) (see the Supplemental Material, Sec. VI [28]). We therefore expect that the emergence of the linear T dependence of the resistivity, as well as the doping dependence of its slope, should be directly related to the precise form of the corresponding scaling function. Indeed, at high temperature and close

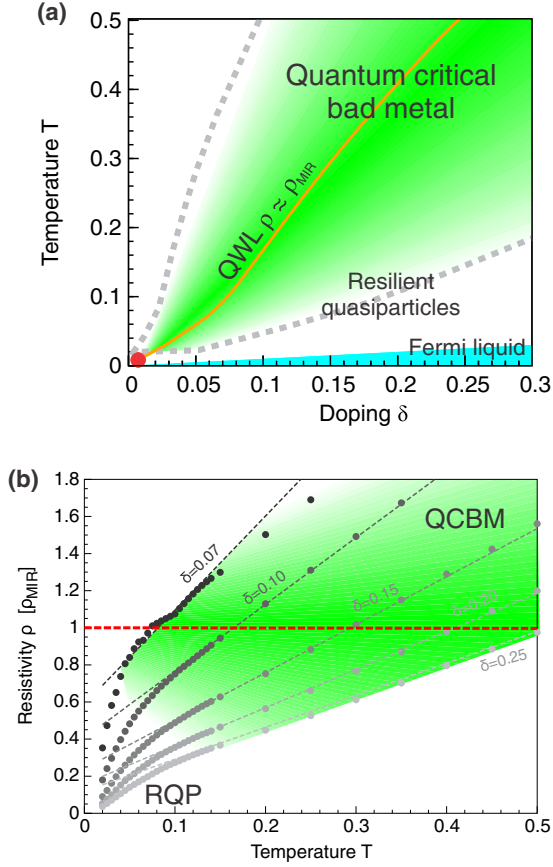


FIG. 3 (color online). (a) DMFT phase diagram of the doped Mott insulator on a frustrated lattice. The bad-metal (green) region matches perfectly the region of quantum critical scaling. (b) The bad-metal regime features linear temperature dependence of resistivity with the slope roughly proportional to an inverse power law of doping which we find to be a consequence of underlying quantum criticality.

to the QWL, the argument of the scaling function $x = d\mu/T^{1/z\nu}$ is always small, and the scaling function can be linearized, viz., $\tilde{F}(x) \approx 1 + Ax + \dots$. We find that the coefficient A has the numerical value $A \approx -0.74$. The functional form for $\rho(T)|_\delta$ close to the QWL is then directly determined by the behavior of the scaling parameter $x(T)|_\delta$. We find that $x(T)|_\delta$ is a linear function in a wide range of temperatures around $T^*(\delta)$. Then, close to the QWL, the resistivity is well approximated by a linear function of the form

$$\rho(T)|_\delta \approx \rho^*(\delta) \left\{ 1 + A \frac{\partial x}{\partial T} \Big|_{\delta, T=T^*(\delta)} [T - T^*(\delta)] \right\}. \quad (2)$$

Furthermore, the slope of the scaling argument at the QWL can be expressed as $(\partial x / \partial T)|_{\delta, T=T^*(\delta)} = \{\chi^*(\delta) (dT^*/d\delta) \times [T^*(\delta)]^{1/z\nu}\}^{-1}$, where $\chi^*(\delta) = (\partial \delta / \partial \mu)|_{T=T^*(\delta)}$. Here, we observe that the charge compressibility is nearly constant along the QWL, $\chi^*(\delta) \approx \chi^* = 0.33$ (see the Supplemental Material, Fig. 6 [28]), which may be interpreted as

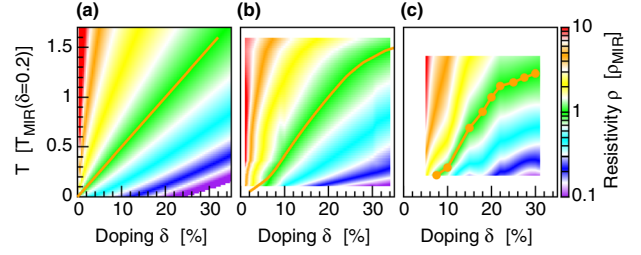


FIG. 4 (color online). Resistivity given by (a) the semianalytical formula obtained from the scaling hypothesis, (b) DMFT result, and (c) the experimental result on cuprate $\text{La}_{2-x}\text{Sr}_x\text{CuO}_4$ samples from Ref. [8].

another manifestation of the quantum critical behavior we identified. $T^*(\delta)$ is approximately a linear function $T^*(\delta) \approx K_0 + K\delta$, where $K \approx 2$ and K_0 is small. In Fig. 3(b), we compare the approximation stated in Eq. (2) with the DMFT result and find excellent agreement.

Finally, noting that for $\delta > 5\%$, $\rho^*(\delta) = \rho_{\text{MIR}}$, we arrive at the central result of this Letter,

$$\rho_{\text{QCBM}}(T)|_\delta \approx \rho_{\text{MIR}} [1 + C\delta^{-1/z\nu} (T - K\delta)]. \quad (3)$$

In the quantum critical bad-metal regime, the resistivity has a linear temperature dependence with the slope decreasing as a power $-1/z\nu$ of doping. This demonstrates a direct connection of the universal high-temperature behavior in the bad-metal regime with the (zero-temperature) quantum phase transition. The MIR limit of the resistivity is reached at temperature roughly proportional to the amount of doping, $T^*(\delta) \propto \delta$, since the doping level sets the main energy scale in the problem. The result of this simplified scaling formula is color-plotted in Fig. 4(a) (with $C = 0.69$, $K = 1.97$, and $z\nu = 1.35$) and shown to capture the features of the full DMFT solution at high temperatures.

Discussion.—Sufficiently systematic experimental studies of doped Mott insulators, covering an appreciable range of doping and temperature, remain relatively scarce. Still, approximately linear temperature dependence of the resistivity at high temperatures with a slope that decreases with doping has been observed, most notably in the seminal work of Takagi *et al.* [8] on $\text{La}_{2-x}\text{Sr}_x\text{CuO}_4$. To make a qualitative comparison with our theory and to highlight a universal link of bad-metal behavior and quantum criticality associated with the Mott metal-insulator transition, in Fig. 4 we color code the reported experimental data; here the temperature is shown in units of T_{MIR} at 20% doping and the resistivity is given in units of ρ_{MIR} , which in this material is estimated as $1.7 \text{ m}\Omega \text{ cm}$. The experimental results presented in Fig. 4(c) cover the temperature range of 150–1000 K at 5% to 30% doping. Here one observes a striking similarity between DMFT theory and the experiment, as already noted in early studies [39–41]. We established this result by focusing on an exactly solvable model, where all ordering tendencies are suppressed, and single-site DMFT becomes exact. Real materials, of course,

exist in finite (low) dimensions where systematic corrections to DMFT need to be included [42–45]. In many cases [46–48], these nonlocal corrections prove significant only at sufficiently low temperatures. Then our findings should be even quantitatively accurate in the high-temperature incoherent regime, as in the very recent experiments on organic materials [49] for the case of half-filling.

We thank E. Abrahams, H. Alloul, S. Hartnoll, N. Hussey, K. Kanoda, A. Schofield, Q. Si, J. Schmalian and M. Vojta for useful discussions. J. V. and D. T. acknowledge support from the Serbian Ministry of Education, Science and Technological Development under Project No. ON171017. V. D. was supported by the NSF, Grants No. DMR-1005751 and No. DMR-1410132. Numerical simulations were run on the AEGIS e-Infrastructure, supported in part by FP7 projects EGI-InSPIRE and PRACE-3IP. J. V., D. T., and M. J. R. acknowledge support from the bilateral French-Serbian PHC Pavle Savic 2012-2013 grant.

-
- [1] S. Sachdev, *Quantum Phase Transitions* (Cambridge University Press, Cambridge, England, 1999).
- [2] H. v. Löhneysen, A. Rosch, M. Vojta, and P. Wölfle, *Rev. Mod. Phys.* **79**, 1015 (2007).
- [3] G. R. Stewart, *Rev. Mod. Phys.* **56**, 755 (1984).
- [4] G. R. Stewart, *Rev. Mod. Phys.* **73**, 797 (2001).
- [5] O. Gunnarsson, M. Calandra, and J. E. Han, *Rev. Mod. Phys.* **75**, 1085 (2003).
- [6] N. E. Hussey, K. Takenaka, and H. Takagi, *Philos. Mag.* **84**, 2847 (2004).
- [7] V. J. Emery and S. A. Kivelson, *Phys. Rev. Lett.* **74**, 3253 (1995).
- [8] H. Takagi, B. Batlogg, H. L. Kao, J. Kwo, R. J. Cava, J. J. Krajewski, and W. F. Peck, *Phys. Rev. Lett.* **69**, 2975 (1992).
- [9] V. Dobrosavljević, N. Trivedi, and J. M. Valles, Jr., *Conductor-Insulator Quantum Phase Transitions* (Oxford University Press, New York, 2012).
- [10] M. M. Qazilbash, K. S. Burch, D. Whisler, D. Shrekenhamer, B. G. Chae, H. T. Kim, and D. N. Basov, *Phys. Rev. B* **74**, 205118 (2006).
- [11] A. W. Tyler, A. P. Mackenzie, S. NishiZaki, and Y. Maeno, *Phys. Rev. B* **58**, R10107 (1998).
- [12] P. Limelette, P. Wzietek, S. Florens, A. Georges, T. A. Costi, C. Pasquier, D. Jérôme, C. Mézière, and P. Batail, *Phys. Rev. Lett.* **91**, 016401 (2003).
- [13] F. Kagawa, K. Miyagawa, and K. Kanoda, *Nature (London)* **436**, 534 (2005).
- [14] J. Merino, M. Dumm, N. Drichko, M. Dressel, and R. H. McKenzie, *Phys. Rev. Lett.* **100**, 086404 (2008).
- [15] M. M. Qazilbash, J. J. Hamlin, R. E. Baumbach, L. Zhang, D. J. Singh, M. B. Maple, and D. N. Basov, *Nat. Phys.* **5**, 647 (2009).
- [16] A. Georges, G. Kotliar, W. Krauth, and M. J. Rozenberg, *Rev. Mod. Phys.* **68**, 13 (1996).
- [17] H. Terletska, J. Vučićević, D. Tanasković, and V. Dobrosavljević, *Phys. Rev. Lett.* **107**, 026401 (2011).
- [18] J. Vučićević, H. Terletska, D. Tanasković, and V. Dobrosavljević, *Phys. Rev. B* **88**, 075143 (2013).
- [19] V. Dobrosavljević, E. Abrahams, E. Miranda, and S. Chakravarty, *Phys. Rev. Lett.* **79**, 455 (1997).
- [20] A. Camjayi, R. Chitra, and M. J. Rozenberg, *Phys. Rev. B* **73**, 041103 (2006).
- [21] X. Deng, J. Mravlje, R. Žitko, M. Ferrero, G. Kotliar, and A. Georges, *Phys. Rev. Lett.* **110**, 086401 (2013).
- [22] A. Donos and S. A. Hartnoll, *Nat. Phys.* **9**, 649 (2013).
- [23] S. Hartnoll, [arXiv:1405.3651](https://arxiv.org/abs/1405.3651).
- [24] P. Werner, A. Comanac, L. de Medici, M. Troyer, and A. J. Millis, *Phys. Rev. Lett.* **97**, 076405 (2006).
- [25] K. Haule, *Phys. Rev. B* **75**, 155113 (2007).
- [26] E. Gull, A. J. Millis, A. I. Lichtenstein, A. N. Rubtsov, M. Troyer, and P. Werner, *Rev. Mod. Phys.* **83**, 349 (2011).
- [27] G. Kotliar, S. Murthy, and M. J. Rozenberg, *Phys. Rev. Lett.* **89**, 046401 (2002).
- [28] See Supplemental Material at <http://link.aps.org/supplemental/10.1103/PhysRevLett.114.246402>, which includes Refs. [29–33], for numerical details, determination of T_c and quantum Widom line, and scaling analysis.
- [29] D. S. Fisher, G. Kotliar, and G. Moeller, *Phys. Rev. B* **52**, 17112 (1995).
- [30] M. J. Rozenberg, R. Chitra, and G. Kotliar, *Phys. Rev. Lett.* **83**, 3498 (1999).
- [31] M. J. Case and V. Dobrosavljević, *Phys. Rev. Lett.* **99**, 147204 (2007).
- [32] M. Jarrell and J. E. Gubernatis, *Phys. Rep.* **269**, 133 (1996).
- [33] A. W. Sandvik, *Phys. Rev. B* **57**, 10287 (1998).
- [34] R. Žitko, D. Hansen, E. Perepelitsky, J. Mravlje, A. Georges, and B. S. Shastry, *Phys. Rev. B* **88**, 235132 (2013).
- [35] P. Werner and A. J. Millis, *Phys. Rev. B* **75**, 085108 (2007).
- [36] A. Amaricci, G. Sordi, and M. J. Rozenberg, *Phys. Rev. Lett.* **101**, 146403 (2008).
- [37] P. Nozières, *Eur. Phys. J. B* **6**, 447 (1998).
- [38] G. G. Simeoni, T. Bryk, F. A. Gorelli, M. Krisch, G. Ruocco, M. Santoro, and T. Scopigno, *Nat. Phys.* **6**, 503 (2010).
- [39] T. Pruschke, D. L. Cox, and M. Jarrell, *Phys. Rev. B* **47**, 3553 (1993).
- [40] M. Jarrell and T. Pruschke, *Phys. Rev. B* **49**, 1458 (1994).
- [41] The high-temperature slope of the resistivity curves is estimated to be proportional to δ^{-1} in Ref. [40]. However, only four doping levels were considered and having in mind the uncertainty of the analytical continuation, it is difficult to distinguish this value from our slope $\delta^{-1/z\nu} = \delta^{-1/1.35}$. Our numerical data are in agreement with high precision CTQMC data from Ref. [21].
- [42] T. Maier, M. Jarrell, T. Pruschke, and M. H. Hettler, *Rev. Mod. Phys.* **77**, 1027 (2005).
- [43] G. Kotliar, S. Y. Savrasov, K. Haule, V. S. Oudovenko, O. Parcollet, and C. A. Marianetti, *Rev. Mod. Phys.* **78**, 865 (2006).
- [44] G. Sordi, P. Sémon, K. Haule, and A.-M. S. Tremblay, *Phys. Rev. B* **87**, 041101 (2013).
- [45] E. Gull, O. Parcollet, and A. J. Millis, *Phys. Rev. Lett.* **110**, 216405 (2013).
- [46] A. Georges, *Ann. Phys. (Berlin)* **523**, 672 (2011).
- [47] D. Tanasković, K. Haule, G. Kotliar, and V. Dobrosavljević, *Phys. Rev. B* **84**, 115105 (2011).
- [48] J. Kokalj and R. H. McKenzie, *Phys. Rev. Lett.* **110**, 206402 (2013).
- [49] T. Furukawa, K. Miyagawa, H. Taniguchi, R. Kato, and K. Kanoda, *Nat. Phys.* **11**, 221 (2015).